ANNUAL REVIEWS

Combining Modern and Paleoceanographic Perspectives on Ocean Heat Uptake

Geoffrey Gebbie

Department of Physical Oceanography, Woods Hole Oceanographic Institution, Woods Hole, Massachusetts 02543, USA; email: ggebbie@whoi.edu

ANNUAL REVIEWS CONNECT

www.annualreviews.org

- Download figures
- Navigate cited references
- Keyword search
- Explore related articles
- Share via email or social media

Keywords

ocean circulation, climate change, planetary energy balance, deglaciation, Medieval Climate Anomaly, Little Ice Age

Abstract

Monitoring Earth's energy imbalance requires monitoring changes in the heat content of the ocean. Recent observational estimates indicate that ocean heat uptake is accelerating in the twenty-first century. Examination of estimates of ocean heat uptake over the industrial era, the Common Era of the last 2,000 years, and the period since the Last Glacial Maximum, 20,000 years ago, permits a wide perspective on modern-day warming rates. In addition, this longer-term focus illustrates how the dynamics of the deep ocean and the cryosphere were active in the past and are still active today. The large climatic shifts that started with the melting of the great ice sheets have involved significant ocean heat uptake that was sustained over centuries and millennia, and modern-ocean heat content changes are small by comparison.

1. INTRODUCTION

Monitoring Earth's energy imbalance is key for estimating the strength of anthropogenic forcing and for projecting how the world will warm in the twenty-first century and beyond. Solar radiation represents a large incoming energy flux at the top of the atmosphere ($342 \, \text{W} \, \text{m}^{-2}$), but it is nearly balanced by reflected shortwave ($\sim 107 \, \text{W} \, \text{m}^{-2}$) and outgoing longwave ($\sim 235 \, \text{W} \, \text{m}^{-2}$) radiation (e.g., Peixoto & Oort 1992). To determine the effects of anthropogenic activity, Earth's energy imbalance must be estimated with an accuracy of approximately $0.1 \, \text{W} \, \text{m}^{-2}$ (e.g., Von Schuckmann et al. 2016). For the available observational methods, inference of Earth's energy imbalance at this level is challenging. Satellite observations allow the determination of monthly top-of-atmosphere energy flux anomalies to a precision of $\pm 0.17 \, \text{W} \, \text{m}^{-2}$ at 95% confidence, but the absolute value is uncertain to $\pm 4 \, \text{W} \, \text{m}^{-2}$ due to calibration issues (Loeb et al. 2018). Constraints based on thermal expansion or direct constraint of the surface energy budget are no more accurate (Meyssignac et al. 2019). Estimates of the changing inventory of stored energy within the climate system are presently the only viable candidate for providing a sufficient empirical constraint on Earth's energy imbalance (e.g., Johnson et al. 2016), although such an approach can be complemented by other methodologies.

Attention has focused on the oceans because they are thought to have stored more than 90% of the excess heat resulting from emissions of greenhouse gases (Trenberth et al. 2016). For example, the oceans are estimated to have stored 93% of the energy that resulted from the planetary imbalance for 1955–2010 (Levitus et al. 2012). By contrast, the cryosphere and atmosphere stored much less of the excess energy, currently thought to be 3% and 1%, respectively. While 93% is often cited as the unchanging oceanic energy contribution, the partitioning among the Earth system components is expected to change over time, with a nearly one-to-one ratio during the last deglaciation (Bereiter et al. 2018b). Furthermore, high-quality temperature observations have not been available over the entire modern warming era.

The uncertainty in modern-day upper-ocean heat uptake has been reported to be as small as $0.01 \, \text{W} \, \text{m}^{-2}$ when put into terms of an equivalent top-of-atmosphere heat flux (Balmaseda et al. 2013). Much of the confidence comes from the similar time evolution of recent estimates (Domingues et al. 2008, Cheng et al. 2017, Ishii et al. 2017), but note that the estimates are not independent because of their use of similar input data sets. The interpretations of instrumental records, including those originating from bottle samples, bathythermographs, CTD (conductivity, temperature, and depth) devices, and profiling floats, have been updated over time. Therefore, integral measures of ocean heat content must account for potential systematic offsets resulting from the evolving mix of available instruments (e.g., Willis et al. 2007, Abraham et al. 2013) and spatially heterogeneous biases (e.g., Kennedy et al. 2011, Chan et al. 2019). Some of the issues with time-evolving data networks are alleviated by focusing on the past 15 years, where Global Ocean Ship-Based Hydrographic Investigations Program (GO-SHIP) global repeat hydrographic data (Talley et al. 2016) and the Argo profiling float program (Lyman et al. 2010) provide a more complete sample of the global ocean. In this more restricted time interval, the upper-ocean heat uptake rate has been estimated as $0.61 \pm 0.09 \, \text{W} \, \text{m}^{-2}$ for the upper 1,800 m (Johnson et al. 2016). A more recent estimate arrived at a result within those error bars (Cheng et al. 2017). The uncertainty in upper-ocean heat uptake has decreased significantly in the last decade as additional observations have been gathered (e.g., compare with Loeb et al. 2012), but the deep ocean has not seen the same type of improvement, and these estimates do not account for some types of errors (Meyssignac et al. 2019).

To more accurately assess the planetary energy imbalance, we require information about energy storage in the entire ocean. Studies have estimated that the deep ocean (below 2,000 m) takes

up 10% (Zanna et al. 2019), 16% (Purkey & Johnson 2010), or 19% (Church et al. 2011) of the upper-ocean warming. Changes in abyssal circulation have been hypothesized to result in the increased heat content of the Southern Ocean [e.g., see the review by Purkey et al. (2018)]. The uncertainty of global (top-to-bottom) ocean heat content is certainly much larger due to limitations in models and observations in the denser water classes of the polar, mid-depth, and abyssal oceans. For example, the Coupled Model Intercomparison Project Phase 5 (CMIP5) coupled climate models underestimate heat uptake in the Southern Ocean (Durack et al. 2014), implying as much as a 20% revision to the planetary heat imbalance. Quasi-global observational sampling by thousands of Argo profiling floats has been available since about 2005 (e.g., Wijffels et al. 2016), but these floats do not measure below 2,000-m depth. Thus, temperature and salinity are rarely measured by in situ instruments over approximately half of the ocean's volume. The deep ocean is the second largest energy reservoir in the climate system after the upper ocean, and understanding the response of this deep reservoir requires a focus on longer timescales.

This review seeks to put the most recent ocean heat uptake estimates of 0.5–0.7 W m^{-2} into the context of longer (multidecadal to millennial) timescales. Such timescales put a wider perspective on present-day heat uptake. In addition, the dynamics of these longer timescales may still have some expression today. This research direction leads to the long temperature time series of paleoceanographic proxies that predate the instrumental record. Ocean heat uptake over the last deglaciation (∼20,000–10,000 years ago) and the Common Era (previous two millennia) will serve as examples to explore the longer-timescale dynamics of ocean heat uptake.

2. BACKGROUND

2.1. Mechanisms of Ocean Heat Uptake

Reconstructing the detailed evolution of air–sea heat fluxes is difficult in the satellite era (e.g., Clayson & Bogdanoff 2013) and is only more difficult for previous eras, which rely solely on data from in situ instruments and paleoceanographic proxies. When considering the magnitude of solar radiation, it is unsurprising that fluxes across the sea surface are the dominant mechanism for ocean heat uptake. Integration of the first law of thermodynamics over the oceanic volume, however, yields three types of contributions (e.g., Warren 2006): (*a*) boundary and radiative fluxes across the sea surface (F_{sfc}), (*b*) geothermal fluxes across the seafloor (F_{bot}), and (*c*) the dissipation of mechanical energy (ϵ). While some authors consider only air–sea heat fluxes to contribute to ocean heat uptake, this article takes the broader view that all three contributions are part of heat uptake, and reviews the latter two contributions next.

2.1.1. Geothermal heat. Geothermal flux due to lithospheric cooling of the seafloor is often ignored in modern oceanographic studies despite a global input rate of approximately 30 TW. Geothermal heat flux is a function of the age of the lithosphere, with young regions contributing more than 250 mW m^{-2} and older regions decreasing to 30 mW m^{-2} (Stein & Stein 1994). A gridded global map of geothermal fluxes yielded a mean value of 86 mW m^{-2} (Emile-Geay & Madec 2009). Geothermal heat fluxes are smaller than typical air–sea fluxes, but they persistently heat the ocean. The global-mean geothermal flux is approximately 15% of the modern-ocean warming estimated by Johnson et al. (2016).

2.1.2. Dissipation of mechanical energy. Sources of mechanical energy to the ocean include the tides, winds, biology, and pressure loading. The tides input 3.5 TW (Munk & Wunsch 1998), and winds input 1 TW to the large-scale geostrophic circulation and 2 TW to the Ekman drift

(Ferrari & Wunsch 2009). Biological mixing is an uncertain but potentially large contributor, with a plausible power estimate of 1 TW (Dewar et al. 2006). The power input by pressure loading is a small contributor according to an analysis of data from the Topography Experiment/Positioning, Ocean, Solid Earth, Ice Dynamics, Orbital Navigator (TOPEX/POSEIDON) altimeter (0.04 TW; Wang et al. 2006). Mechanical energy is either directly dissipated by the molecular viscosity of seawater or converted to potential energy through turbulent diffusion (e.g., Lueck & Reid 1984, St. Laurent & Simmons 2006). Approximately 0.3–0.4 TW goes into maintaining the abyssal stratification, but Wunsch & Ferrari (2004) noted that no global integral of warming by dissipation is available. Here, we examine the order of magnitude of this quantity using a global model. A best estimate of total dissipation from a model with parameterized internal tides is 3.49 TW (Jayne & St. Laurent 2001). The integrated dissipation varies in the vertical, with $50 \, \mathrm{mW \, m^{-2}}$ in the upper ocean, decreasing to $1 \, \mathrm{mW \, m^{-2}}$ in the deep ocean, and increasing again to $5 \, \mathrm{mW \, m^{-2}}$ near the seafloor. The global integral of ocean warming from dissipation of mechanical energy is equivalent to a top-of-atmosphere energy imbalance of $5 \, \mathrm{mW \, m^{-2}}$. This global effect is approximately 1% of the modern warming estimated by Johnson et al. (2016).

There is a great deal of additional power input to the sea surface, such as the estimated 60-TW power input to surface waves [see the review by Ferrari & Wunsch (2009)]. If some fraction of this energy is not dissipated on beaches, then it must be removed by surface waves or other processes in the open ocean. For this reason, the estimate of $5 \, \mathrm{mW \, m^{-2}}$ may be a severe underestimate of ocean heating by dissipation of mechanical energy. Another unresolved issue is the decomposition of mechanical energy between marginal seas and the open ocean. Over long timescales, the total amount of dissipation in the open ocean can change due to the exposure of marginal seas and continental shelves (Arbic et al. 2004, Schmittner et al. 2015).

2.2. Thermodynamics of Ocean Heat Uptake

It would be of great practical use to have a measurable internal ocean quantity that permits the accounting of ocean heating. One goal is to define an oceanic quantity for the heat content per mass of seawater, h, such that changes in the mass-weighted integral of this quantity, defined as $\Delta\mathsf{H}$, are related to ocean heat uptake. The average rate of ocean heat uptake over a time interval, Δt, is then

$$\frac{\Delta\mathsf{H}}{\Delta t} \equiv \frac{\Delta(\overline{\rho\mathsf{h}}V)}{\Delta t} \approx Q_{\mathrm{sfc}} + Q_{\mathrm{bot}} + Q_\epsilon, \qquad\qquad 1.$$

where the overline is a volumetric average over volume, V. The terms Q_{sfc} and Q_{bot} are defined as the time-averaged products of the boundary flux and the relevant area (i.e., $Q_{\mathrm{sfc}} = \langle F_{\mathrm{sfc}} A_{\mathrm{sfc}} \rangle$, $Q_{\mathrm{bot}} = \langle F_{\mathrm{bot}} A_{\mathrm{bot}} \rangle$). Warming by dissipation of mechanical energy is $Q_\epsilon = \langle \overline{\rho\epsilon} V \rangle$.

Enthalpy is often used as a thermodynamic variable that accounts for heating, but enthalpy changes when water sinks or rises. Such an effect cannot be distinguished from heating by air–sea fluxes. Instead, potential enthalpy has been put forward as the best candidate for h because it accounts for these pressure changes by comparing all water parcels at a surface reference pressure, as is done for potential temperature (McDougall 2003) (see the sidebar titled Potential Enthalpy). Potential enthalpy is calculated by integrating the product of seawater density, ρ, and the specific potential enthalpy, h^0, over the oceanic volume, V. This diagnostic is constructed to properly account for air–sea fluxes by using a surface reference pressure, but geothermal fluxes act at a variety of pressures and cannot be referenced simultaneously. Thus, potential enthalpy is a very good, but imperfect, measure of ocean heat uptake. (Such imperfections are unlikely to be observationally detectable.)

Potential enthalpy is a thermodynamic state variable completely described by salinity, temperature, and pressure. Salinity observations, however, are more difficult to make and do not have the same coverage as temperature. To test the influence of salinity, we approximate the heat content by $h^\theta \equiv c_p^0 \theta$ and $H^\theta \equiv \rho_0 \overline{h^\theta} V$, with a fixed seawater density ($\rho_0 = 1,026.7$ kg m^{-3}) and specific heat capacity ($c_p^0 \approx 3,992$ J kg^{-1} K^{-1}) and a spatially variable potential temperature, θ. The squared spatial correlation between ρh^0 and $\rho_0 h^\theta$ in the World Ocean Circulation Experiment climatology (Gouretski & Koltermann 2004) is greater than 0.99. Thus, the spatial distribution of heat content is not substantially degraded by missing information about salinity, although systematic offsets are not tested for in the correlation analysis.

2.3. The Expected Frequency Spectrum of Ocean Heat Uptake

The major problem addressed by this review is how well ocean heat uptake can be inferred from noisy, sparse measurements of the internal state of the ocean. Uncertainties in ocean heat uptake may be quantified by understanding the timescales of heat uptake variability. Long time series of temperature from paleoceanographic proxies indicate that the frequency spectrum of surface temperature is a power law (e.g., $f^{-\beta}$; Zhu et al. 2019), and the high latitudes follow an exponent of $\beta = 1.64 \pm 0.04$ until the exponent decreases at centennial and higher frequencies (Huybers & Curry 2006). This red spectrum indicates that temperature contains autocovariance that permits any given data point to have a predictive capability at times both before and after the observation was taken. This section attempts to link this temperature variability to the spectral character of ocean heat uptake by surface boundary fluxes.

We first link temperature, a dynamical variable that affects the ocean circulation, to the analysis of passive tracers in order to set statistical expectations. The tracer concentration at an interior point is related to a surface time series, $b(t)$, by a boundary Green's function, $G(t, \tau)$:

$$c(t) = \int_0^\infty G(t, \tau) b(t - \tau) d\tau, \qquad 2.$$

where $G(t, \tau)$ is often called the transit time distribution (e.g., Deleersnijder et al. 2001, Haine & Hall 2002), τ is a time lag, and the distribution has a finite width due to ocean mixing and the multiplicity of pathways from the surface to the interior ocean (e.g., Khatiwala et al. 2001, Waugh et al. 2003). The function also depends on time for a nonsteady ocean circulation (Haine et al. 2008). The Green's function is interpreted as the distribution of transit times since the various elements composing a fluid parcel were at the surface. The global-mean tracer value can also be related to the sea surface by integrating over these functions:

$$\bar{c}(t) = \int_0^\infty G_m(t, \tau) b(t - \tau) d\tau, \qquad 3.$$

where G_m is the mass-weighted global average of G [i.e., $G_m(t, \tau) = \overline{\rho \, G(t, \tau)}/\overline{\rho}$]. According to both general circulation models and radiocarbon observations, the form of $G_m(t, \tau)$ for today's

ocean has a maximum value at zero lag with a tail that decreases exponentially to zero at several thousand years, consistent at first order with a one-dimensional leaky pipe (Mouchet & Deleersnijder 2008). The long tail indicates that the global-mean tracer value depends on surface conditions many hundreds of years prior.

The mean ocean potential temperature, $\bar{\theta}(t)$, is related to the mean sea-surface temperature (SST), $\theta_b(t)$, with a similar form,

$$\bar{\theta}(t) = \int_0^\infty \left[G_p(t, \tau) + G_a(t, \tau, \theta) \right] \theta_b(t - \tau) d\tau, \qquad 4.$$

but where we introduce a function that is not temperature dependent [i.e., the passive function, $G_p(t, \tau)$] and one that is actively affected by temperature through density and circulation change, $G_a(t, \tau, \theta)$. In this more complete case, the relationship between SST and global-mean temperature may no longer be linear. The histories of $G_p(t, \tau)$ and $G_a(t, \tau, \theta)$ are difficult to quantify because they involve long timescales that predate the instrumental era, but models suggest that the response of global-mean temperature to SST is nearly linear when considering centennial timescales (Marshall et al. 2015, Zanna et al. 2019). An intermediate-complexity model run over a longer, 800-year time interval does imply a significant contribution by $G_a(t, \tau, \theta)$, however (Scheen & Stocker 2020). To make progress, we substitute a passive, time-invariant function, $G_m(\tau)$, for the terms inside the square brackets of Equation 4 in order to set statistical expectations for ocean heat uptake.

When random SST time series are used to force a steady circulation model described by the function $G_m(\tau)$, the resulting evolution of global-mean temperature is a filtered version of the forcing. At periods longer than 10,000 years, the frequency spectrum of $\bar{\theta}$ converges to the SST spectrum, indicating that the ocean is a low-pass filter (**Figure 1**). Energy at millennial and higher frequencies is attenuated by the ocean circulation, however, leading to mean ocean temperature following a power law that is steeper (i.e., $f^{-2.1}$) than that at the surface. Thus, oceanic temperature distributions inherently contain autocovariance that is useful for statistically infilling gaps in sparse data.

Ocean heat uptake is proportional to temperature differences over time. SST variability has a red frequency spectrum with more energy at low frequencies, but the spectrum of ΔT diagnosed with a time interval of 5 years is not expected to be dominated by low frequencies to the same extent. At periods longer than 500 years, the ΔT spectrum has a slope that is shifted to be shallower by an exponent of two, as follows from the Fourier differentiation theorem (Bracewell 1986). At centennial and higher frequencies, the roll-off of the SST spectrum leads to a ΔT spectrum that is white or blue, with equal or greater energy at high frequencies relative to low frequencies. We expect ocean heat uptake to have a similar character, where an observation of ocean heat uptake for any 5-year interval may not be representative of longer-term averages.

The statistical expectation shown here assumes that surface climate changes are globally uniform, but this is a poor assumption given the interhemispheric variability shown in ice and marine sediment cores, including evidence for a bipolar seesaw. In addition, we have assumed that the modern-day circulation well describes the past ocean, but ocean properties were undoubtedly different during glacial times. In some paleoceanographic cases, it would not be surprising for the rate of ocean response to be halved or doubled (e.g., Muglia et al. 2018), leading to modifications in the frequency spectra presented here. The dominance of the red temperature spectrum over five orders of magnitude, however, suggests that the basic picture presented here will still hold as new data become available. At this point, errors in paleoceanographic age models will have to be improved before the frequency spectra can be directly corroborated (e.g., Lin et al. 2014).
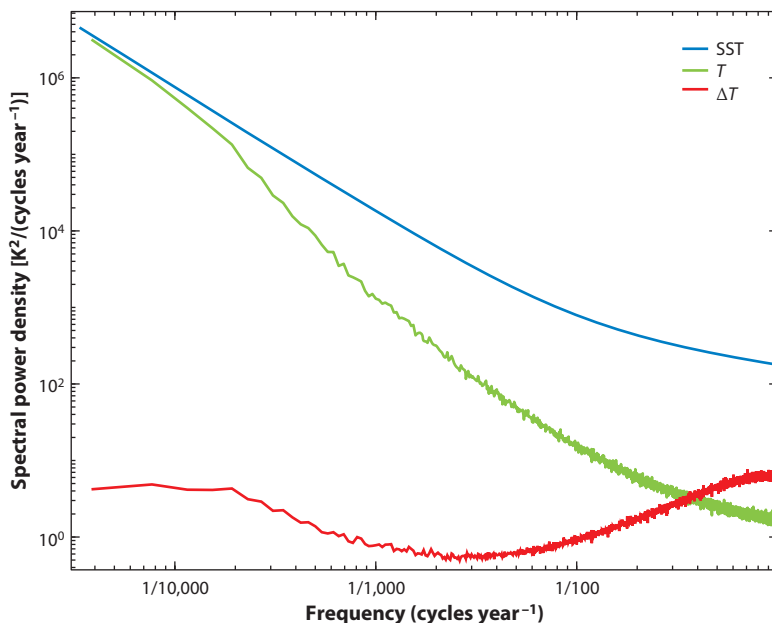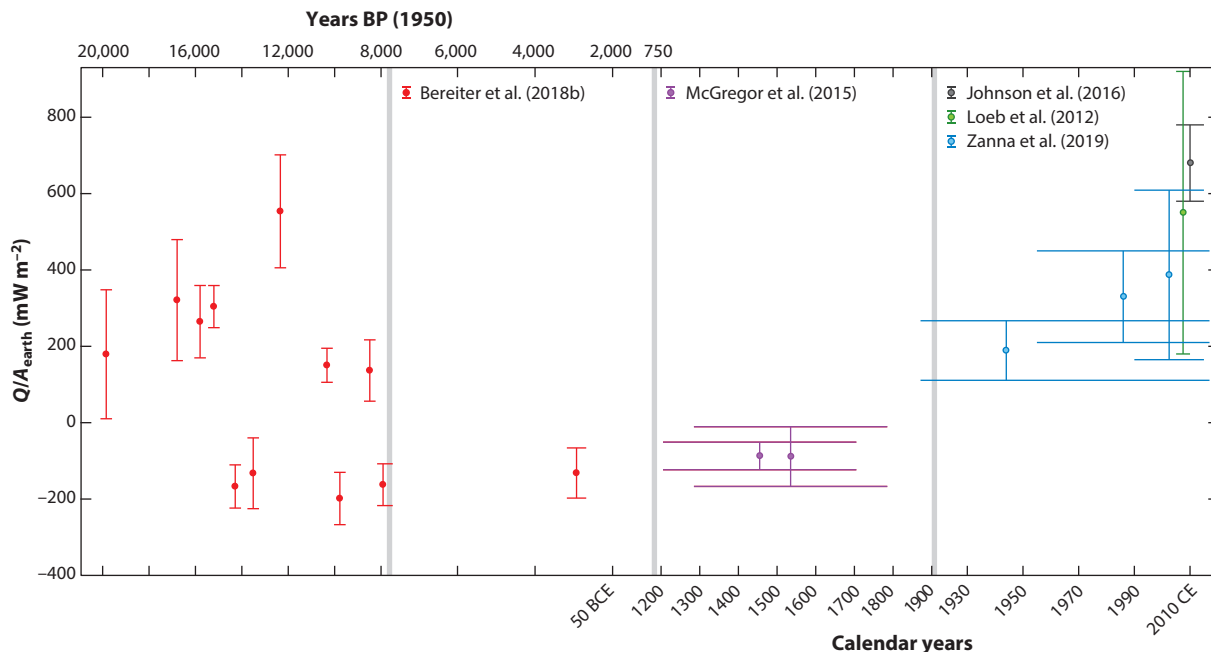
Figure 1

Frequency spectrum of high-latitude SST (*blue*) (Huybers & Curry 2006); global-mean ocean temperature (*T*), as computed by convolution with $G_m(\tau)$ from Gebbie & Huybers (2012) (*green*); and the global-mean temperature difference over a five-year interval [i.e., $\Delta T = \bar{\theta}(t+5) - \bar{\theta}(t)$] (*red*). Frequency spectra were estimated by averaging 100 random realizations. Abbreviation: SST, sea-surface temperature.

2.4. The Power-Law Estimate of Ocean Heat Uptake

Later, this review surveys data sets related to ocean heat uptake, such as various temperature observations. These observations, however, require additional interpretation to infer ocean heat uptake. To aid in interpreting the observations, and to draw conclusions that link observations over different timescales, we develop a statistical estimation technique based on the expected power-law description from the previous section. Here, we assume that the spectral power of SST in 3,000 frequency bands, with periods ranging from 10 to 30,000 years, is known from work by Huybers & Curry (2006). Observations and their error estimates are then used to determine the phase of SST variability for each frequency, such that we obtain the SST evolution consistent with the power-law behavior of Earth's climate and temperature observations.

A power-law description permits climate variability on disparate timescales to be compared with a common framework. Next, we draw on examples from the last deglaciation, the Common Era, and the modern warming era to review what is known about ocean heat uptake. The resulting spectral description illustrates that ocean heat uptake has varied greatly over the last 20,000 years and that its uncertainty depends strongly on the time interval of averaging, as shown in **Figure 2**. The remainder of this review details the information in this figure.

The power-law estimate will necessarily be incomplete, as we focus on using observations that are especially well suited for constraining the global ocean, but many regional time series are not reviewed here [see the review by Rosenthal et al. (2017)]. Observational constraints in the power-law estimate are not restricted to SST, but we additionally exploit the connection between global-mean SST and mean ocean temperature that is described by a boundary Green's function in Equation 4. We assume that the Green's function has the simple form given by Mouchet &

Figure 2

Global ocean heat uptake from the Last Glacial Maximum to 2017 CE. Observationally derived estimates of global ocean heat uptake are expressed as an equivalent planetary energy imbalance (*circles*) with 2σ uncertainty bounds (error bar height in *y* direction) and averaging interval (error bar width in *x* direction). Only events statistically distinguishable from zero at the 90% confidence level are shown. Ocean heat uptake estimates are from Johnson et al. (2016) (*black*), Loeb et al. (2012) (*green*), and Zanna et al. (2019) (*blue*). Data from McGregor et al. (2015) (*purple*) and Bereiter et al. (2018b) (*red*) were used to produce a power-law estimate of heat uptake. For clarity, the scaling of the time axis is adjusted at 1920 CE, 1200 CE, and 8,000 years BP (*gray bars*). Abbreviation: BP, before present.

Deleersnijder (2008): $G_m(\tau) = (1/q)\exp(-\tau/750 \text{ years})$, where q is the proper normalizing constant. No regional variations or changes in circulation are explicitly handled by the power-law estimate, so our goal is restricted to understanding basic principles of ocean heat uptake.

3. THE LAST DEGLACIATION

What is the average net heat flux into the ocean necessary to transition from a glacial state to an interglacial state? The arguments above suggest that changes in mean ocean temperature contain information to address this question. The goal is to put the current state of knowledge into the context of the basic concepts and statistics outlined above.

3.1. Deglacial Temperature Observations

This section reviews recent information about deglacial ocean temperature change from the Last Glacial Maximum [LGM, i.e., 24,000–18,000 years before present (24–18 kyr BP)] to the modern day.

3.1.1. Foraminiferal records. Long time series of oxygen-isotope ratios, principally the δ^{18}O of planktonic and benthic foraminifera (e.g., Emiliani 1955, Shackleton et al. 1977), have been used to infer the waxing and waning of the great ice sheets; however, the δ^{18}O of calcite contains

the signal of both ice volume and the temperature in which the foraminiferal shells calcified (e.g., Shackleton 1974, Marchitto et al. 2014). One additional piece of information, the seawater $\delta^{18}O$ ratio, is needed to extract the temperature signal.

Independent estimates of deep-ocean temperature have been produced by analysis of the Mg/Ca ratio of benthic (e.g., Sosdian & Rosenthal 2009, Elderfield et al. 2012) and planktonic (e.g., Shakun et al. 2015) foraminiferal shells. Benthic foraminiferal $\delta^{18}O$ was then split into a seawater $\delta^{18}O$ signal and a temperature change of $T_{HOL} - T_{LGM} = 3 \pm 1°C$ (Elderfield et al. 2012), where T_{HOL} and T_{LGM} are the early Holocene (11.5–7 kyr BP) and LGM temperatures, respectively. The Mg/Ca ratio is affected by carbonate saturation effects (e.g., Martin et al. 2002), however, and more recent studies suggest that Mg/Li ratios may be more reliable (Bryan & Marchitto 2008, Marchitto et al. 2018, Umling et al. 2019).

Global compilations of $\delta^{18}O$ and Mg/Ca have been produced in order to better estimate global ocean heat content. A compilation of 80 proxy records, including terrestrial records (Shakun et al. 2012), estimated a 3.5°C global surface temperature change from the LGM (defined here as 22–19 kyr BP) to the Holocene (11–7 kyr BP). This global surface temperature change is larger than global-mean SST change detected in marine proxy records (Shakun et al. 2015), as expected due to the smaller heat capacity of land relative to the ocean.

One complication of comparing estimates of deglacial temperature change is the definition of the LGM. The LGM is reflected as an extreme value in marine sediment cores and is sometimes reported as this snapshot in time. Ice sheets, however, reached their maximum extent at different times around the world (e.g., Clark et al. 2009), and there is a time lag between temperature and ice-volume change (Waelbroeck et al. 2002). As the time intervals for the LGM and Holocene are not standard, the definition used by each work is included here.

3.1.2. Pore-water measurements. The history of past $\delta^{18}O$ change leaves an imprint in the pore fluids of the seafloor sediment (e.g., McDuff 1985, Schrag et al. 1996). When pore-water $\delta^{18}O$ is paired with benthic foraminiferal $\delta^{18}O$, a temperature signal can be recovered via a paleotemperature equation (e.g., Marchitto et al. 2014). Recovery of the past temperature evolution involves deconvolving signals that have diffused downward into the sediment (Miller et al. 2015). The results are sensitive to uncertain deep sediment conditions (Wunsch 2016), and the resulting uncertainties in temperature inferences likely approach 1°C.

Pore-water measurements indicate deglacial (LGM to Holocene) warming of approximately 4°C in the North Atlantic, as inferred from the Bermuda Rise and Feni Drift, and 2°C in the South Pacific and South Atlantic (Adkins et al. 2002). These temperature changes are consistent with an ocean circulation model with northern source water (i.e., the glacial analog of North Atlantic Deep Water) that was 4°C colder during glacial times and southern source water that cooled 1.5°C to near the freezing point (Gebbie 2012). The implied water-mass distribution is also consistent with benthic foraminiferal $\delta^{18}O$ at the pore-water locations and other abyssal sites.

The inversion described by Gebbie (2012) infilled the gaps between the pore-water data locations and added additional data to produce a globally gridded map of the deglacial temperature evolution. LGM-to-Holocene ocean temperature change was diagnosed as 2.6°C, where the Southern Hemisphere pore-water data have more influence on global-mean temperature because Antarctic water masses fill more of the world ocean than North Atlantic waters (Gebbie & Huybers 2011). A simple analysis for the uncertainty in the estimate is as follows: The fraction filled by Antarctic water masses is unclear, and a 20% uncertainty leads to a standard error of $\pm0.4°C$. Temperature changes above the thermocline contribute an uncertainty of approximately 0.4°C, because they represent nearly 20% of the world ocean by mass and have a plausible error of $\pm2°C$. A plausible estimate is thus $2.6 \pm 0.6°C$.

3.1.3. State estimates and inversions.

LGM state estimates have combined much of the LGM temperature and other paleoceanographic observations with general circulation models. These state estimates produce a gridded estimate of temperature, finding that LGM mean SST was 1.9°C (Breitkreuz et al. 2019), 2°C (Amrhein et al. 2018), or 2.2°C (Kurahashi-Nakamura et al. 2017) cooler than modern SST, which is consistent with the 1.9 ± 1.8°C cooling in the Multiproxy Approach for the Reconstruction of the Glacial Ocean Surface (MARGO) compilation used to constrain the estimates (Waelbroeck et al. 2009). The LGM mean ocean temperature was reported as 1.2°C cooler than the modern temperature (Breitkreuz et al. 2019), a small value that may be symptomatic of the difficulty in running general circulation models for the long time periods necessary to bring the deep ocean into quasi-equilibrium with the surface. In addition, alkenone-based SST records used in MARGO tend to indicate warmer LGM temperatures than other proxies (Kurahashi-Nakamura et al. 2017), which may also explain why the state estimates infer a smaller deglacial change.

Problems with the slow equilibration time of the deep ocean are handled with a steady-state inversion method that produces equilibrated fields by construction (Gebbie 2014). Three inversions produced by this method are discussed in detail below. They included various data constraints, such as several hundred benthic foraminiferal $\delta^{18}O$ and $\delta^{13}C$ measurements, but the dynamical constraints are less sophisticated than the state estimates. Inferred LGM-to-modern temperature changes are bounded by 1–4°C at all depths. The vertical structure has little similarity among the reconstructions, however, suggesting that the sparse data of the LGM pose an ongoing challenge for reconstructing the spatial temperature distribution.

3.1.4. Noble-gas measurements.

Noble-gas measurements from trapped ice-sheet bubbles appear to constrain mean ocean temperature changes with higher precision than the previous methods because the averaging of many interior ocean data points is not necessary (Bereiter et al. 2018a). Noble gases record the integral effect of a well-mixed atmosphere undergoing adjustment to the temperature-dependent oceanic saturation state. Noble-gas records are only minimally affected by diffusive smoothing in the firn column (Mitchell et al. 2011), and thus the ratio of noble gases can be related to the mean ocean temperature. The West Antarctic Ice Sheet (WAIS) Divide ice core is especially advantageous because of a difference between gas age and ice age of approximately 200 years in the Holocene, rising to a maximum of 500 years at the LGM. The noble-gas analysis method indicates a global-mean oceanic temperature change of 2.57 ± 0.24°C from the LGM (22–18 kyr BP) to the Holocene (11.5–7.5 kyr BP) (Bereiter et al. 2018b). The method has also been used to infer that the last interglacial was 1.0 ± 0.3°C warmer than the modern temperature (Shackleton et al. 2020).

An intermediate-complexity ocean model suggests that the noble gases have high precision (±0.3°C) in tracking mean ocean temperature when interior ocean properties are near saturation values (Ritz et al. 2011). Other uncertainties can arise due to age-scale uncertainty and the assumed evolution of sea-level rise. Additionally, the analysis method assumes that there are no internal heat sources or sinks in the ocean. If geothermal heat is passed through the ocean at a constant rate, then the impact on the analysis is small, but deglacial ocean circulation changes likely modify the rate of passage of geothermal heat to the atmosphere. Due to the difference between gas age and ice age (Buizert et al. 2015), modern warming is not yet reflected in sealed ice-core bubbles and thus may not be used to calibrate the records.

3.2. Comparing Temperature Observations

Foraminiferal and pore-water observations permit an inference of temperature change based on local observations. Noble-gas observations are instead related to the global-mean oceanic changes.

These observational differences lead to biases in the inferred deglacial warming, which we take into account next.

The Holocene global-mean temperature can be expressed as a mass-weighted average,

$$\bar{\theta}_{HOL} = \frac{M_{lid}\bar{\theta}_{HOL}^{lid} + M_{int}\bar{\theta}_{HOL}^{int}}{M_{lid} + M_{int}},$$ 5.

where the overline refers to a spatial average, and the superscript refers to the averaging over some depth layer. We divide the ocean into two layers: the interior, below approximately 130-m modern-day water depth, which also existed during the LGM, and the meltwater lid, which is the uppermost 130 m of the modern ocean. The modern-day oceanic masses in these layers are M_{int} and M_{lid}, respectively. The overline without any label is the global average. The mean LGM temperature is simply the average over the interior layer, $\bar{\theta}_{LGM} = \bar{\theta}_{LGM}^{int}$. Foraminiferal and pore-water measurements are giving a sample of $\bar{\theta}_{HOL}^{int} - \bar{\theta}_{LGM}^{int}$, the temperature difference between two points in the interior. On the other hand, noble gases provide information about the mean ocean temperature change, $\bar{\theta}_{HOL} - \bar{\theta}_{LGM}$, which is not the same quantity because it is not restricted to the interior layer.

The definitions above permit the distinction to be quantified. The mean ocean temperature change is expanded as

$$\bar{\theta}_{HOL} - \bar{\theta}_{LGM} = \bar{\theta}_{HOL}^{int} - \bar{\theta}_{LGM}^{int} + \frac{M_{lid}}{M_{lid} + M_{int}}\left(\bar{\theta}_{HOL}^{lid} - \bar{\theta}_{HOL}^{int}\right),$$ 6.

where the second term on the right-hand side is an offset that can be calculated with available modern-ocean information. The prefactor of this term has a value of approximately 1/40, and the modern temperature difference between the lid and the interior is approximately 16°C. Thus, the global-mean temperature difference should be offset 0.4°C higher than pointwise samples at the same seafloor location. Another issue is that any given seafloor location is not a good sample of the global mean.

3.3. Translating Deglacial Temperature Change to Heat Uptake

This section considers inferring deglacial ocean heat uptake from temperature observations. The difference in ocean heat content between the LGM and the Holocene is given, at lowest order, by expanding Equation 1:

$$\Delta H = (\Delta\overline{\rho h})V + \overline{\rho h}\Delta V + \dots,$$ 7.

where any approximation for h can be used, and the ellipsis represents higher-order terms. Defining the change in oceanic mass as $\Delta M = \Delta(\bar{\rho}V)$ gives

$$\Delta H \approx (\Delta\bar{h})M + \bar{h}\Delta M,$$ 8.

where this is an approximation. The average of h in the second term depends on an arbitrary baseline state, and thus ΔH is also arbitrary whenever the ocean mass changes, such as during the deglaciation. The arbitrariness is evident when using the h^{θ} definition for heat content and changing the temperature scale.

The arbitrariness of the calculation is removed when considering two quantities that have the same mass. One way forward is to consider the heat content of the glacial ocean together with the meltwater from the ice sheets, which together have the same mass as the modern ocean. Equation 8 then reduces to

$$\Delta H \approx (\Delta\bar{h})M + (\bar{h} - h_F)\Delta M,$$ 9.

where the heat content of the fresh water is $h_F \Delta M$. The equation is an approximation owing to higher-order differences between volume-weighted and mass-weighted averaging. Now all h values are expressed as differences in Equation 9, and the arbitrariness is removed. The value ΔH should now be interpreted as all heat uptake by the ocean or by fresh water that is routed to the ocean.

The energy required to melt ice would not be included in the heat content calculation of Equation 9. The heat uptake by melting ice is

$$\Delta H_{ice} = (\overline{h_F} - \overline{h_{ice}})\Delta M, \qquad\qquad 10.$$

where the heat content difference between ice and fresh water takes into account the latent heat of melting.

The ocean inversions described in Section 3.1.3 estimate both temperature and salinity and therefore permit the calculation of potential enthalpy, h^0. The deglacial ocean heat uptake is then given by differencing Holocene and LGM values:

$$\Delta H^0 = \overline{\rho_{HOL} h^0_{HOL}}V_{HOL} - \overline{\rho_{LGM} h^0_{LGM}}V_{LGM} - h^0_F \Delta M, \qquad\qquad 11.$$

where the third term on the right-hand side eliminates any arbitrariness in the definition. The potential enthalpy of fresh water does not vanish when calculated using the Gibbs seawater toolbox (IOC et al. 2010). For the 4.7×10^{19} kg of deglacial freshwater, the thermodynamic energy is approximately 3×10^{21} J. The implied planetary energy imbalance is much less than 1 mW m^{-2} over the deglaciation, however, and can be safely ignored.

Inferences from noble gases are interpreted as changes in mean ocean potential temperature (Bereiter et al. 2018b). If we approximate heat content by h^θ from Section 2, then Equation 11 is modified as

$$\Delta H^\theta = \rho_0 c_p^0 (\overline{\theta_{HOL}}V_{HOL} - \overline{\theta_{LGM}}V_{LGM}), \qquad\qquad 12.$$

where $\theta_F = 0°C$ and one term is eliminated. The error in assuming that mean density and specific heat capacity are constant over the deglaciation is 0.1% and 0.2%, respectively, when considering the additional pressure and dilution of salinity by meltwater, although we do not have information about regional variations. If foraminiferal and pore-water inferences are assumed to be well calibrated (i.e., nondrifting), then temperature may be substituted for θ in Equation 12. Temperature and potential temperature are not identical over the deglaciation, as the sea-level rise of 130 m leads to a small but systematic temperature increase of approximately 0.01°C without any potential temperature effect. The difference is less than 1% of the deglacial ocean's mean temperature change and is approximately 5% of the smallest published errors on this quantity. Caution is warranted, however, because temporal changes in the observational network can transfer the uncertainty in the absolute value of mean ocean temperature to estimates of heat uptake (Wunsch 2016).

3.4. Average Deglacial Ocean Heat Uptake

The deglacial heat uptake rate is calculated for four deglacial ocean reconstructions according to the approximations of Section 3.3. The estimates are then divided by Earth's surface area to facilitate comparison with the implied planetary energy imbalance (**Table 1**). Benthic foraminiferal data regarding temperature changes at a fixed location are translated to changes in mean ocean temperature according to Section 3.2.

Deglacial ocean uptake estimates vary from 12,000 to 20,000 ZJ (1 ZJ $\equiv 10^{21}$ J) and represent an awesome amount of energy that dwarfs the excess energy stored during the modern warming era by a factor of at least 20. The noble-gas-derived estimate has the smallest uncertainty,

Table 1 Quantities related to deglacial ocean heat uptake

Study	$\overline{\theta_{HOL} - \theta_{LGM}}$ (°C)	$\overline{\theta}_{HOL} - \overline{\theta}_{LGM}$ (°C)	ΔH (ZJ)[a, b]	Q/A_{earth} (mW m^{-2})[b]
Bereiter et al. 2018b	2.17 ± 0.24[b]	2.57 ± 0.24	$15,600 \pm 1,500$	99 ± 9
Elderfield et al. 2012[c]	3.0 ± 1.0	3.4 ± 1.0[b]	$20,000 \pm 6,000$	130 ± 40
Gebbie 2012	2.6 ± 0.6	3.0 ± 0.6	$18,000 \pm 3,000$	110 ± 20
Gebbie 2014[c, d]	1.6–2.2	2.0–2.6	12,000–16,000	70–100

For each study, this table shows, from left to right, the differences between Holocene mean ocean temperature and LGM mean ocean temperature, the mean temperature differences for a time series at a fixed location, the LGM-to-Holocene changes in heat content, and the average deglacial ocean heat uptake. Abbreviation: LGM, Last Glacial Maximum.

[a] 1 ZJ $\equiv 10^{21}$ J.

[b] Not diagnosed in the original work but inferred in this review.

[c] Heat uptake rate assumes a 10,000-year deglacial interval.

[d] Modern (1990s) minus LGM value, assuming no heat uptake in the Holocene; the range of values comes from the two inversions in Gebbie (2014) and inversion #2 in Gebbie et al. (2015).

15,600 ± 1,500 ZJ, as a direct result of the small uncertainty in mean ocean temperature. It is also reassuring that this estimate falls near the center of the other estimates and is within the large errors of the benthic foraminiferal estimate of Elderfield et al. (2012).

Despite the huge change in ocean heat content, the average deglacial heat uptake rate is just 10–20% of modern values taken during the era of the Argo program (e.g., Johnson et al. 2016). The deglaciation differs from the modern era in that the deep ocean had time to come into quasi-equilibrium with the surface, and therefore much of the thermodynamic energy is stored at great depth.

Deglacial-average heat uptake rates are estimated to be anywhere from 70 to 130 mW m^{-2}, with a best estimate of 99 ± 9 mW m^{-2}, when put into the context of a planetary energy imbalance by dividing by Earth's surface area. These values are not significantly different than the mean geothermal heating through the seafloor of 87 mW m^{-2} (Emile-Geay & Madec 2009). The passage of geothermal heat to the atmosphere is mediated by the ocean circulation (Joyce 1986, Adcroft et al. 2001), and thus circulation changes are expected to alter the oceanic storage of geothermal heat (Adkins et al. 2005). It is unclear to what degree the deglacial-mean heat uptake can be explained by geothermal heat.

3.5. Time Evolution of Deglacial Heat Uptake

Here, we invert noble-gas observations for the phase of deglacial SST variability. We apply each noble-gas observation as a constraint on mean ocean temperature over a 50-year averaging interval. The resulting power-law estimate includes a deglacial time series of global-mean SST, mean ocean temperature, and ocean heat uptake that fills the gaps in the data in accordance with a minimum variance estimate (Wunsch 1996). The method is analogous to objective mapping in spectral coordinates (Bretherton et al. 1976), where the result is consistent with the oceanic frequency spectrum.

Deglacial ocean warming occurred in a first step around 18–15 kyr BP, followed by a second step around 13–12 kyr BP (**Figure 3a**). Noble-gas observations are consistent with the expected power-law behavior, with greater variability at millennial and lower frequencies. Mean ocean temperature is well constrained throughout the last deglaciation relative to the early Holocene, where a lack of data leads to uncertainties in mean ocean temperature of ±1°C. Additional data, such as compilations of SST data (e.g., Shakun et al. 2012), would be a natural choice to fill this gap.
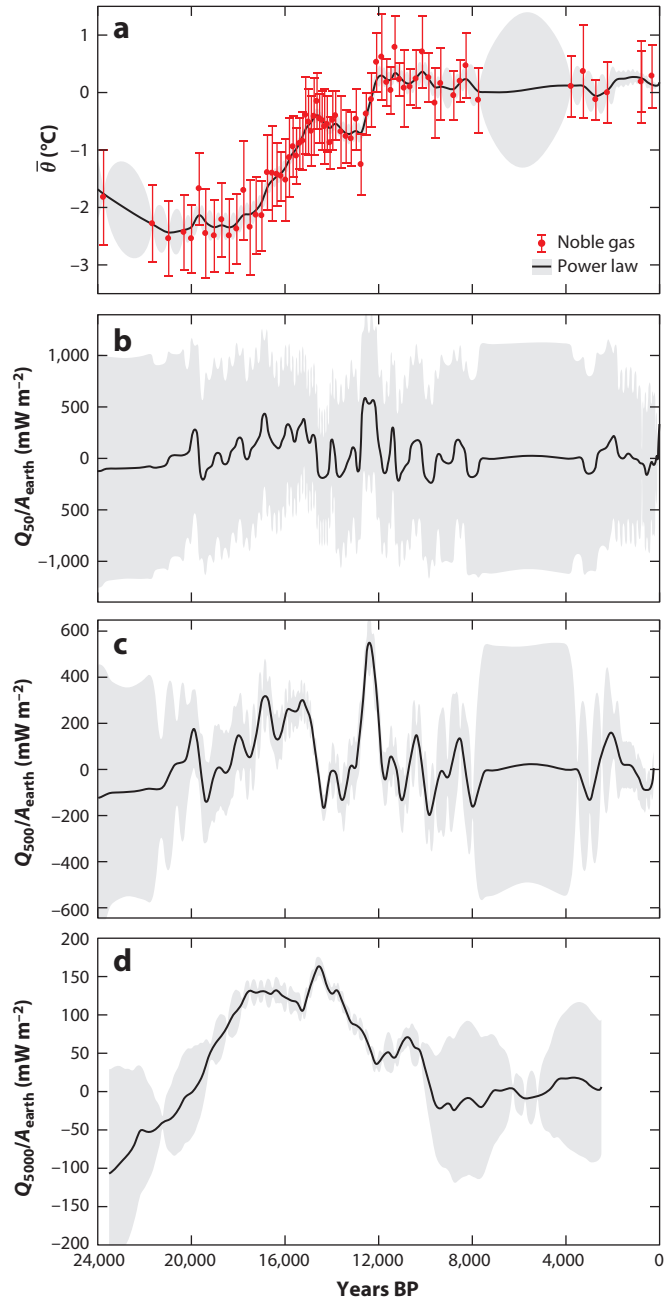
Figure 3

The last deglaciation. (*a*) Deglacial evolution of mean ocean temperature from noble-gas measurements (*red circles*, with 2σ error bars) and a power-law estimate (*black line*, with 2σ errors shown in *gray*), referenced to global-mean SST in 1870. (*b–d*) Average ocean heat uptake (*black lines*, with 2σ errors shown in *gray*) over a running 50-year interval (panel *b*), 500-year interval (panel *c*), and 5,000-year interval (panel *d*) in terms of an equivalent planetary energy imbalance. Abbreviations: BP, before present; SST, sea-surface temperature.

The evolution of Antarctic surface temperature is highly correlated with mean ocean temperature as inferred from noble gases (Parrenin et al. 2013, Brook & Buizert 2018). Both time series lack the centennial-scale variability seen in carbon dioxide and methane in the WAIS Divide core (Marcott et al. 2014). It is surprising that mean ocean temperature and Antarctic surface temperature could be highly correlated without any temporal lag, as any signals imparted on Antarctic Bottom Water would take at least hundreds of years to penetrate the world ocean (Primeau 2005). This conundrum may be resolved with shifts in age models or with a mechanism by which the deep ocean actively influences the Antarctic continent.

Figure 3 shows mean ocean temperature and the solution variance through time, but such information is not sufficient to calculate both ocean heat uptake and its uncertainty. A range of temperature uncertainty may indicate that long-term trends are well known but higher frequencies are not, or vice versa. In the deglaciation, the oceanic power-law behavior implies that much of the uncertainty comes from the unknown phasing of high-frequency variability, and the average heat flux over 50-year time intervals has an uncertainty at the 2σ level that approaches 1,000 mW m^{-2} (**Figure 3b**). The power-law estimate of heat uptake is not greater than 500 mW m^{-2}, a value less than the uncertainty. Consequently, the energy in high frequencies generally precludes our ability to resolve deglacial heat uptake at 50-year timescales that are statistically distinguishable from zero at the 95% confidence level.

Statistically significant ocean heat uptake can be detected when the temporal resolution is restricted to 500-year intervals. One example is at the start of the Younger Dryas. Differences of the noble-gas data would suggest a heat uptake of 1,500 mW m^{-2} at 12.7 kyr BP, which is twice as large as warming rates in the early twenty-first century. These large rates may not be trustworthy, however, due to alteration of the WAIS Divide ice core by bubble-clathrate transformation (Shackleton et al. 2019). The Taylor Glacier on Antarctica does not have clathrates, and instead puts the peak Younger Dryas ocean heat uptake at 600–700 mW m^{-2}. Heat uptake of 1,500 mW m^{-2} is not supported by the statistics of the WAIS Divide data, either. Instead, we find a heat uptake of 550 ± 150 mW m^{-2} over a 500-year interval at the start of the Younger Dryas, once possible high-frequency contamination is taken into account. This heat uptake is fast enough to rival anthropogenic warming and was sustained for several centuries.

Increases in ocean heat uptake have been noted to coincide with times where Pa/Th ratios were low in the North Atlantic (Baggenstos et al. 2019). Disruptions to the Atlantic meridional overturning circulation (AMOC) have been put forward to explain both. General circulation models suggest that AMOC disruptions cause the ocean to warm (Galbraith et al. 2016). In particular, ocean heat loss by deep convection is suppressed during these disruptions, leading to a net heat uptake by other mechanisms (Palter et al. 2014). Ocean heat uptake by AMOC disruption is hypothesized to be as large as 400 mW m^{-2}. The last deglaciation included sustained 5,000-year intervals where heat uptake was statistically nonzero (**Figure 3d**), and it is unclear whether shorter disruptions of the circulation can explain the whole signal.

3.6. Energy Required to Melt Ice

In the modern warming era, ice melt consumes only 3% of the excess energy in the Earth system (Gleckler et al. 2016). Such a fraction may be the average over the modern warming period but may not have held in recent decades (Berger et al. 2017). The details of this decomposition likely depend on the geometrical configuration of the ice sheets and their marine margins (Levermann et al. 2013).

Because the geometrical configuration of the ice sheets varied over the last deglaciation, it is worth recomputing the energy required to melt 130 m of grounded ice. The latent heat of melting

can be found by comparing the enthalpy of fresh water and ice (Curry & Webster 1999). The latent heat is affected by less than 1% by pressure, and therefore it is inconsequential for our purposes whether the ice sheets melted from above or below (Feistel & Wagner 2005, 2006). Salt has a minor effect of 1% or less on latent heat as well (Warren 2006, Huang 2010). Here, we find that 15,770–15,830 ZJ of energy is needed to melt ice, depending on the amount of ice needed to raise sea level in light of seawater density changes (Simms et al. 2019). This equipartition of energy between ice melt and ocean heat uptake has been recently noted by other authors (Lambeck et al. 2014, Bereiter et al. 2018b). Due to the near equipartition, ocean heat uptake cannot be equated to the planetary energy imbalance during the deglaciation.

4. THE COMMON ERA

The last 2,000 years were climatically quiescent relative to the last deglaciation, but the Common Era still hosted long-term climate variations prior to the industrial era (e.g., Oppo et al. 2009). Data compilations from the Past Global Changes 2k (PAGES2k) project include terrestrial and ice-core data (Emile-Geay et al. 2017). Atmospheric data assimilation techniques have been used to reconstruct the Medieval Climate Anomaly (MCA) around 1000 CE (e.g., Hakim et al. 2016). Marine proxy data compiled by the Ocean2k project (McGregor et al. 2015) indicate a global cooling trend after the peak of the MCA that reached its nadir over roughly the years 1400–1800, a period known as the Little Ice Age (LIA) (Paasche & Bakke 2010).

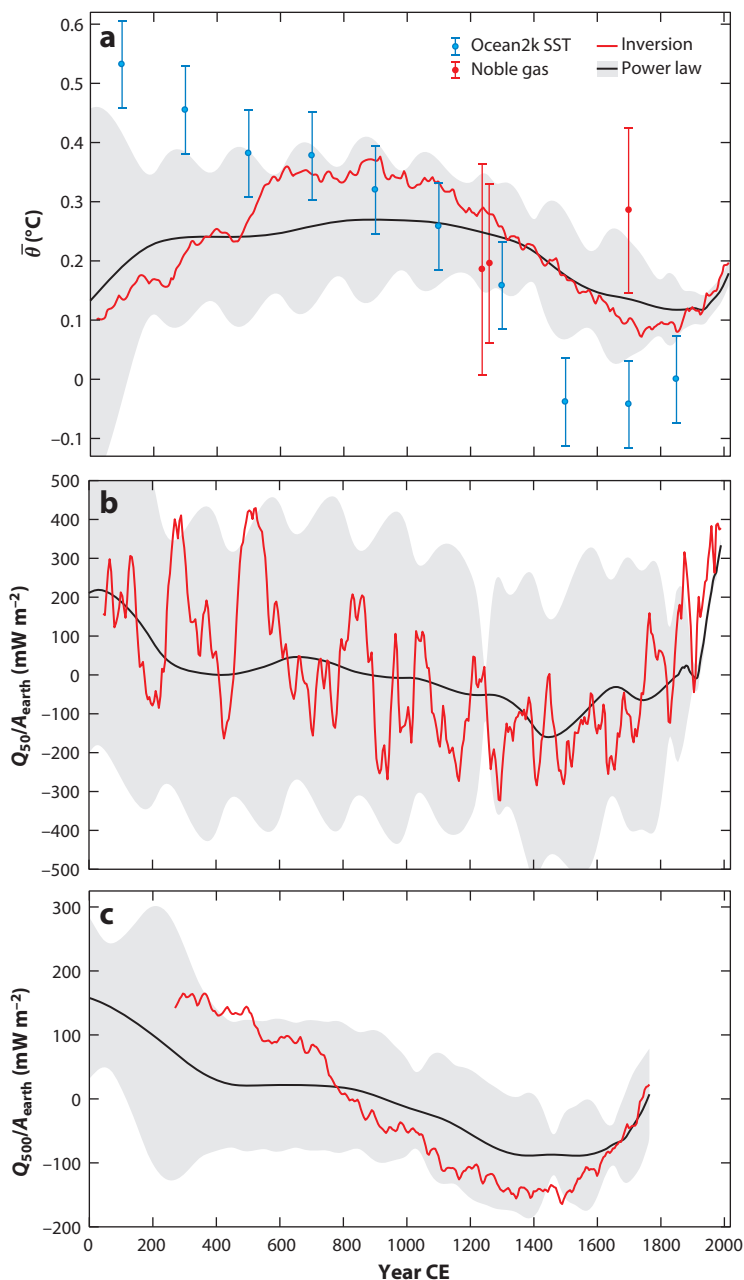### 4.1. Common Era Evolution of Mean Ocean Temperature

The Ocean2k global-mean SST compilation is derived from 57 marine proxy records that, in aggregate, show a statistically significant cooling trend from 700 to 1700 CE over the MCA–LIA transition. The data compilation contains a time series of 200-year averages that have been nondimensionalized. Here, we dimensionalize the values with the recommended values of McGregor et al. (2015) to obtain temperature anomalies, and the inferred global-mean surface cooling over the MCA–LIA transition is near the high end of the expected 0.4–0.6°C range (**Figure 4a**).

Information about the subsurface ocean response to surface anomalies, as encapsulated in the boundary Green's function, permits basic conclusions to be drawn about the evolution of Common Era mean ocean temperature from Ocean2k SST. In addition, the assumption of power-law behavior in the frequency spectrum of SST is used to statistically describe variability at frequencies higher than the 200-year averages of Ocean2k. Here, we apply the Ocean2k SST to our power-law estimate with assumed 2σ errors of 0.3°C, which should be considered optimistic in light of biases incurred by dimensionalizing the product.

Mean ocean temperature is expected to have an MCA–LIA cooling trend that is smaller than SST given the lagged, damped response of the interior ocean. A plausible estimate is ocean cooling of approximately 0.15°C over the interval of 900–1900 CE (black lines in **Figure 4**), but the power-law-derived errors in MCA mean ocean temperature are large, at ±0.2°C (2σ). The uncertainty in Common Era mean ocean temperature displays an undulating pattern due to the 200-year averages of Ocean2k SST, and increasing values in the first millennium of the Common Era.

One realization of the Common Era was produced by an inversion that attempted to reconstruct the three-dimensional evolution of oceanic temperature anomalies over the last 2,000 years (Gebbie & Huybers 2019). The inversion fits an empirical ocean circulation model to modern-day tracer observations, historical temperature observations from the HMS *Challenger* expedition of 1872–1876 (Murray 1895), and the global-mean Ocean2k SST. The resulting ocean temperature evolution is dominated by the propagation of surface climate anomalies from the MCA and LIA

Figure 4

The Common Era. (*a*) The evolution of Ocean2k SST (*blue circles*, with $\sigma/2$ error bars) and mean ocean temperature, $\bar{\theta}$, as inferred from noble-gas measurements (*red circles*, with $\sigma/2$ error bars), the Gebbie & Huybers (2019) Common Era inversion (*red line*), and a power-law estimate (*black line*, with 2σ error shown in *gray*), referenced to global-mean SST in 1870. (*b,c*) Average ocean heat uptake over a running 50-year interval (panel *b*) and a 500-year interval (panel *c*) plotted from the Gebbie & Huybers (2019) inversion (*red line*) and a power-law estimate (*black line*, with 1σ error shown in *gray*). Heat uptake is expressed in terms of an equivalent planetary energy imbalance. Abbreviation: SST, sea-surface temperature.

into the subsurface ocean, where the propagation is coherent for several centuries (red line in **Figure 4***a*). Although the Gebbie & Huybers (2019) inversion was not constrained with oceanic power laws, the resulting mean ocean temperature is consistent with a power-law estimate over the Common Era.

Early-twenty-first-century SST may already be warmer than MCA SST, but it is less likely that modern mean ocean temperature has surpassed MCA values. From the Gebbie & Huybers (2019) inversion, it was inferred that the MCA ocean stored 1,000 ZJ more than the ocean of the year 2000, and that the ~500 ZJ of heat uptake during the modern warming era is just one-third of what is required to reach MCA levels. Amplification of the high-latitude SST signal relative to the global mean can produce a greater MCA–LIA mean ocean cooling, which explains the greater MCA heat content relative to the present day. When considering the range of Common Era scenarios consistent with a power law, however, some cases are admitted where the MCA and the present day have similar oceanic heat content.

4.2. Ocean Heat Loss in the Little Ice Age

It is unclear from **Figure 4***a* whether the MCA–LIA transition was an interval of sustained ocean heat loss or simply a time when years with ocean cooling outnumbered those with heating. Ocean heat uptake that is diagnosed consistently with both the Ocean2k SST data and oceanic power-law behavior indicates that the answer is a function of timescale. Like the last deglaciation, average ocean heat uptake over 50-year intervals is dominated by energetic high-frequency variations, where ocean heating cannot be ruled out during the LIA (**Figure 4***b*). We estimate ocean heat uptake of -100 ± 600 mW m^{-2} (2σ) during the fourteenth and fifteenth centuries, with the large uncertainties reflecting a lack of information about multidecadal and higher-frequency variations. For any given 50-year interval, it is difficult to distinguish heat uptake from zero, as might be expected due to the 200-year average windows of the Ocean2k SST product.

The Gebbie & Huybers (2019) inversion gives one realization of the expected multidecadal and centennial variability in the Common Era that is consistent with our inferences from the power-law estimate. During some 50-year intervals in the LIA, ocean heat uptake switched signs, which is indicative of the ever-present climate variability of the Common Era. At no point during the Common Era is it safe to assume that the ocean was in equilibrium. Strong warming intervals suggest that twentieth-century warming may have had an analog at some point in the earlier Common Era. The Gebbie & Huybers (2019) inversion contains heat uptake of 400 mW m^{-2} for 50 years, and the power-law analysis suggests that heat uptake twice as large is possible. As these values are near the estimated 600–700 mW m^{-2} of early-twenty-first-century warming, we cannot rule out a Common Era analog for modern warming with the specific data sets used here.

Despite the high-frequency variations, it is clear that the LIA had pronounced effects on European winters and that the ocean participated in this climate variability (Paasche & Bakke 2010). When considering the longer timescale of 500 years, sustained ocean heat loss in the MCA–LIA transition becomes detectable (**Figure 4***c*). The time interval 1250–1750 CE, for example, has a statistically significant heat loss equivalent to -90 ± 40 mW m^{-2} at the 95% confidence level. Thus, we corroborate the finding that the MCA–LIA cooling is significant, as was detailed in the trend analysis of McGregor et al. (2015), and place bounds on the rate of ocean heat uptake.

Radiative forcing estimates derived from greenhouse gases, aerosols, and clouds (Myhre et al. 2013); solar variability (Steinhilber et al. 2009); and volcanoes (Crowley & Unterman 2013) have been compiled back to 850 CE. The net air–sea flux is equal to the incoming radiation less the excess energy that is radiated to the atmosphere. If we assume that our ocean heat uptake is dominated by air–sea flux, we find low-frequency changes that are similar between our ocean
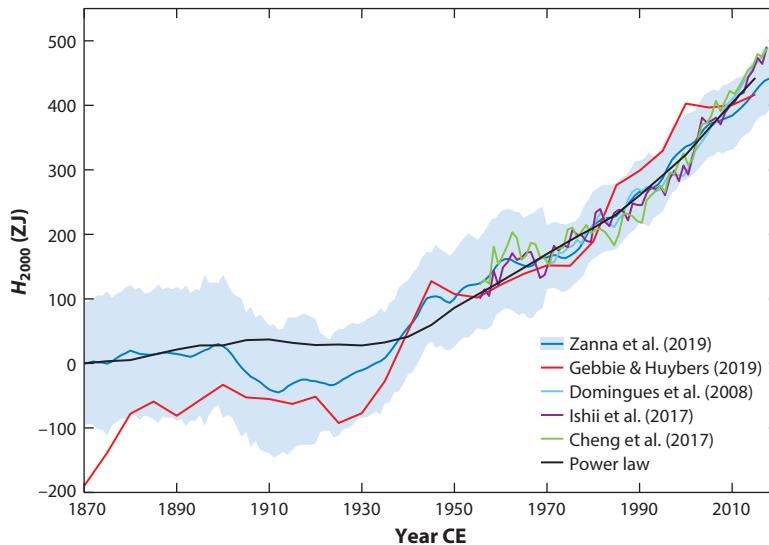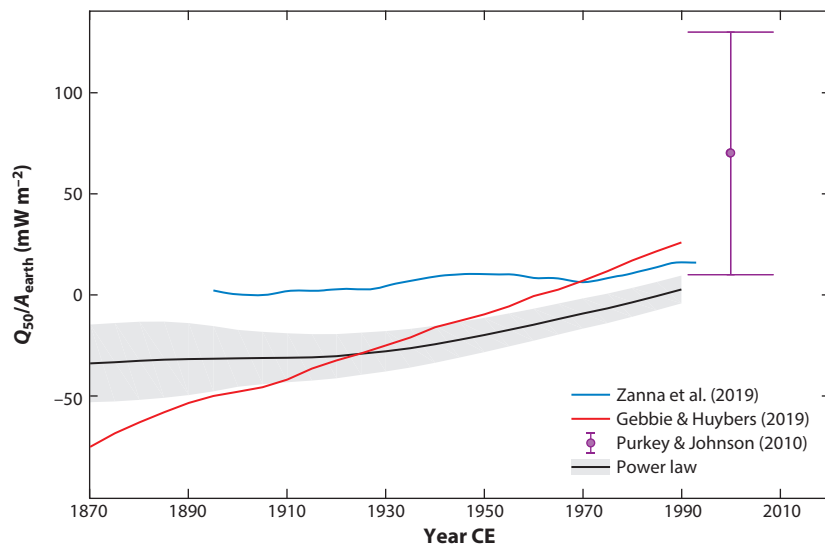
Figure 5

Ocean heat content in the upper 2,000 m, H_{2000}, aligned in the 1990–2005 time interval. The figure shows estimates from Zanna et al. (2019) (*dark blue line*), Gebbie & Huybers (2019) (*red line*), Domingues et al. (2008) (*light blue line*), Ishii et al. (2017) (*purple line*), and Cheng et al. (2017) (*green line*), along with the power-law estimate from this review (*black line*). The baseline value at 1870 and the 2σ error are from Zanna et al. (2019).

diagnostics and independent IPCC estimates of radiative forcing. The reconstructed radiative forcing is somewhat stronger than the observed ocean heat uptake, as is expected for a stable climate with a temperature-dependent back radiation out of the top of atmosphere (e.g., Galbraith et al. 2016).

4.3. Upper-Ocean Heat Uptake During Modern Warming

The period of instrumental oceanography, here defined as 1870 to the present, is relatively data rich compared with the earlier periods of the Common Era. Confidence in our understanding of ocean heat uptake during the modern warming era has been bolstered by the similarity of many different estimates (**Figure 5**). The similarity in estimates is most striking when restricting ocean heat content to the upper 2,000 m and considering times after 1955. Increases in upper-ocean heat uptake over the years 1955–2017 are very similar, including estimates of 330 ± 70 mW m^{-2} (Zanna et al. 2019) and 350 mW m^{-2} (Gebbie & Huybers 2019).

The various estimates of recent upper-ocean heat uptake are not independent, because of their shared use of common input data. A demonstration of the dependence is illustrated by the power-law estimate that is extended from the earlier Common Era. The upper-ocean heat content is closely reproduced by convolving a fixed, global-mean ocean response function with the same Hadley Centre Sea Ice and Sea Surface Temperature (HadISST) 1.1 SST product used to constrain the estimates of Zanna et al. (2019) and Gebbie & Huybers (2019) (black line in **Figure 5**). No regional information about SST or ocean circulation is required. Furthermore, it is not required to consider the dynamical effect of temperature on the circulation, or any circulation changes imposed by external causes. Here, we only require parameterizing the upper-ocean response with an exponentially decaying boundary response function, $G_{2000}(\tau) = (1/q)\exp(-\tau/T^*)$,

Figure 6

Ocean heat uptake below 2,000-m depth, in terms of a planetary energy imbalance, for 50-year averages given by Zanna et al. (2019) (*blue line*), Gebbie & Huybers (2019) (*red line*), and the power-law estimate from this review (*black line*, with 2σ error in *gray*). An observational estimate (*purple*, with 2σ error bar) for 1990–2010 is also included (Purkey & Johnson 2010).

where a best fit is found for $T^* = 125$ years. If ocean heat content estimates are not independent, then the spread of reconstructions may not accurately represent the remaining uncertainty.

To have the power-law estimate fit the other upper-ocean heat content reconstructions so well, additional constraints must hold prior to the instrumental era. The most important is that the Ocean2k SST value for 1900 must be sufficiently similar to SST values from instrumentally based products for the late nineteenth century. Note that the Ocean2k data were produced as an anomaly time series, where mean offsets from modern SST records are statistically possible. If such offsets are allowed, however, then the evolution of early-twentieth-century upper-ocean heat content can be altered outside the bounds depicted in **Figure 5**. The Gebbie & Huybers (2019) inversion permitted and solved for such an offset by blending paleoceanographic and instrumental data during the overlap interval of 1850–1950, giving rise to greater early-twentieth-century warming. This greater warming is supported by the estimated 330 ZJ of ocean warming above 700 m that was inferred from HMS *Challenger* data (Roemmich et al. 2012). These issues emphasize the discrepancies and uncertainties in ocean temperature that still exist in the time period before 1955.

4.4. Deep-Ocean Heat Uptake During Modern Warming

The confidence in upper-ocean heat content during the modern warming era starkly contrasts with the remaining uncertainties in heat content below 2,000-m depth (**Figure 6**). Observational estimates have indicated a deep-ocean heat uptake of 68 ± 61 mW m^{-2} (2σ) when differencing hydrographic sections between 1990 and 2010 (Purkey & Johnson 2010, Desbruyères et al. 2017). Estimation of deep-ocean heat uptake over the entire instrumental era relies to a greater extent on circulation models. Simulations of modern warming that are initialized from equilibrium in 1870 suggest that heat penetrates downward (Gregory 2000) and that average deep-ocean heat uptake is small over 50-year time intervals (Zanna et al. 2019). These estimates would not capture ongoing

trends from the earlier Common Era, if any existed. An inversion that accounts for the LIA found a deep-ocean heat loss of 80 mW m^{-2} early in the modern warming era (Gebbie & Huybers 2019), and our power-law estimate suggests that an even greater cooling is possible, although the uncertainties are large. These discrepancies highlight the ongoing effect that Common Era variability could play in the modern-day ocean. Unfortunately, recent observations do not appear to be sufficient to distinguish between these scenarios, as they all suggest a weak deep-ocean heat uptake in the early twenty-first century.

Deep-ocean cooling could exist as the result of disequilibrium between the upper and deep ocean. Oceanic disequilibrium exists at a range of spatial and temporal scales, from local, short-term variability to longer-term changes that are anticipated to generally have greater spatial extent. Oceanic disequilibrium has been anticipated as a result of the 1815 Tambora (Stenchikov et al. 2009) and 1883 Krakatoa (Gleckler et al. 2006) volcanic eruptions and their lingering effects on energy imbalance. More generally, ocean disequilibrium can result from the differing adjustment times of the interior ocean to surface forcing, where the deep-ocean response may take longer than 1,000 years (e.g., Wunsch & Heimbach 2008). Accordingly, some influence of changes in surface climate over the last millennium is potentially present today. The most isolated waters of the mid-depth Pacific, for example, should still be adjusting to the MCA–LIA transition. In this scenario, these deep waters are cooling, but they are anomalously warm due to the residual influence of the MCA. The role of the circulation in the global average is to move heat from anomalously warm to cold regions, giving rise to an upward heat flux into the upper ocean. For a deep ocean that is 0.1–0.2°C anomalously warm relative to the surface (recall **Figure 4a**) and a heat uptake efficiency of 700 mW m^{-2} K^{-1} (e.g., Dufresne & Bony 2008, Gregory & Forster 2008), a vertical heat flux of 70–140 mW m^{-2} could be explained.

The importance of preindustrial oceanic disequilibrium was evaluated by Gebbie & Huybers (2019) as the difference between a model simulation initialized in 15 CE and 1750 CE. The difference in ocean heat uptake was due to the slow oceanic response to pre-1750 surface conditions. While the ocean heat uptake has a similar pattern of decadal variability in both simulations, there is a systematic offset of −160 mW m^{-2} in the longer Common Era simulation that slowly decreases with time over several centuries. Temperature observations of the 1872–1876 voyage of the HMS *Challenger*, where a statistically significant basin-wide cooling of 0.1°C per century was found between 1,600-m and 2,800-m depth in the Pacific, provide support for a deep ocean in preindustrial disequilibrium.

The degree to which the ocean's long memory affects today's ocean is uncertain due to difficulties in integrating state-of-the-art circulation models over the entire Common Era. An accurate assessment may also require a model that can skillfully predict ocean circulation changes in both the past and the future. The climate history of the Common Era should also be better constrained by recovering additional observations, such as historical subsurface temperature observations and paleoceanographic data. Proper inference of climate sensitivity depends on the past oceanic heat uptake, which this review suggests is tied to the long timescale of deep-ocean dynamics.

SUMMARY POINTS

1. Ocean heat uptake is related to changes in sea-surface temperature and mean ocean temperature, yielding a frequency spectrum with considerable high-frequency energy. This frequency spectrum suggests that 50-year-average ocean heat uptake has a standard deviation greater than 500 mW m^{-2}.

2. Average ocean heat uptake was 150 ± 10 mW m^{-2} from 17,000 to 12,000 years ago, during the last deglaciation, and was punctuated by heat uptake of 550 ± 150 mW m^{-2} from 13,000 to 12,500 years ago, at the start of the Younger Dryas.

3. The ocean cooled at a rate of -90 ± 40 mW m^{-2} over the years 1200–1700, corresponding to the climate transition from the Medieval Climate Anomaly to the Little Ice Age. Inferred variations in heat uptake of ± 400 mW m^{-2} sustained over 50-year intervals indicate that the Common Era climate was never in equilibrium.

4. Upper-ocean heat uptake estimates during the modern warming era can be largely explained by the oceanic response given by a constant circulation to global-mean sea-surface temperature changes, with 50-year average heat uptake rates exceeding 300 mW m^{-2} from 1970 to 2020.

FUTURE ISSUES

1. Observations of mean ocean temperature and global-mean sea-surface temperature set our basic expectations for ocean heat uptake, but utilizing information from regionally distributed proxy data and historical hydrographic data is necessary to decrease the large remaining uncertainties.

2. Existing large-scale data compilations can be explained by the global-mean ocean response, but other explanations that depend on the spatial distribution of sea-surface temperature and ocean circulation changes will be key to understanding the dynamics behind climate variability.

3. Geothermal heat becomes a leading-order contributor to the oceanic heat budget on millennial timescales, suggesting a role that is coupled with ocean circulation change.

4. Improved reconstructions of ocean heat uptake during the modern warming era must address the hidden systematic errors that arise due to the time-evolving composition of the observing system, the sparsity of observations before 1955, and the expected variability of the deep ocean.

DISCLOSURE STATEMENT

ACKNOWLEDGMENTS

LITERATURE CITED

Abraham JP, Baringer M, Bindoff N, Boyer T, Cheng L, et al. 2013. A review of global ocean temperature observations: implications for ocean heat content estimates and climate change. *Rev. Geophys.* 51:450–83

Adcroft A, Scott JR, Marotzke J. 2001. Impact of geothermal heating on the global ocean circulation. *Geophys. Res. Lett.* 28:1735–38

Adkins JF, Ingersoll AP, Pasquero C. 2005. Rapid climate change and conditional instability of the glacial deep ocean from the thermobaric effect and geothermal heating. *Quat. Sci. Rev.* 24:581–94

Adkins JF, McIntyre K, Schrag DP. 2002. The salinity, temperature, and $\delta^{18}O$ of the glacial deep ocean. *Science* 298:1769–73

Amrhein DE, Wunsch C, Marchal O, Forget G. 2018. A global glacial ocean state estimate constrained by upper-ocean temperature proxies. *J. Clim.* 31:8059–79

Arbic BK, MacAyeal DR, Mitrovica JX, Milne GA. 2004. Palaeoclimate: ocean tides and Heinrich events. *Nature* 432:460–60

Baggenstos D, Häberli M, Schmitt J, Shackleton SA, Birner B, et al. 2019. Earth's radiative imbalance from the Last Glacial Maximum to the present. *PNAS* 116:14881–86

Balmaseda MA, Trenberth KE, Källén E. 2013. Distinctive climate signals in reanalysis of global ocean heat content. *Geophys. Res. Lett.* 40:1754–59

Bereiter B, Kawamura K, Severinghaus JP. 2018a. New methods for measuring atmospheric heavy noble gas isotope and elemental ratios in ice core samples. *Rapid Commun. Mass Spectrom.* 32:801–14

Bereiter B, Shackleton S, Baggenstos D, Kawamura K, Severinghaus J. 2018b. Mean global ocean temperatures during the last glacial transition. *Nature* 553:39–44

Berger A, Yin Q, Nifenecker H, Poitou J. 2017. Slowdown of global surface air temperature increase and acceleration of ice melting. *Earth's Future* 5:811–22

Bracewell RN. 1986. *The Fourier Transform and Its Applications*. New York: McGraw-Hill

Breitkreuz C, Paul A, Schulz M. 2019. A dynamical reconstruction of the Last Glacial Maximum ocean state constrained by global oxygen isotope data. *Clim. Past Discuss.* **https://doi.org/10.5194/cp-2019-52**

Bretherton F, Davis R, Fandry C. 1976. A technique for objective analysis and design of oceanographic experiments applied to MODE-73. *Deep-Sea Res.* 23:559–82

Brook EJ, Buizert C. 2018. Antarctic and global climate history viewed from ice cores. *Nature* 558:200–8

Bryan SP, Marchitto TM. 2008. Mg/Ca–temperature proxy in benthic foraminifera: new calibrations from the Florida Straits and a hypothesis regarding Mg/Li. *Paleoceanography* 23:PA2220

Buizert C, Cuffey K, Severinghaus J, Baggenstos D, Fudge T, et al. 2015. The WAIS Divide deep ice core WD2014 chronology – part 1: methane synchronization (68–31 ka BP) and the gas age–ice age difference. *Clim. Past* 11:153–73

Chan D, Kent EC, Berry DI, Huybers P. 2019. Correcting datasets leads to more homogeneous early-twentieth-century sea surface warming. *Nature* 571:393–97

Cheng L, Trenberth KE, Fasullo J, Boyer T, Abraham J, Zhu J. 2017. Improved estimates of ocean heat content from 1960 to 2015. *Sci. Adv.* 3:e1601545

Church JA, White NJ, Konikow LF, Domingues CM, Cogley JG, et al. 2011. Revisiting the Earth's sea-level and energy budgets from 1961 to 2008. *Geophys. Res. Lett.* 38:L18601

Clark P, Dyke A, Shakun J, Carlson A, Clark J, et al. 2009. The Last Glacial Maximum. *Science* 325:710–14

Clayson CA, Bogdanoff AS. 2013. The effect of diurnal sea surface temperature warming on climatological air–sea fluxes. *J. Clim.* 26:2546–56

Crowley TJ, Unterman MB. 2013. Technical details concerning development of a 1200 year proxy index for global volcanism. *Earth Syst. Sci. Data* 5:187–97

Curry J, Webster P. 1999. Ocean surface exchanges of heat and fresh water. *Thermodyn. Atmos. Oceans* 65:247–65

Deleersnijder E, Campin JM, Delhez EJM. 2001. The concept of age in marine modelling I. Theory and preliminary model results. *J. Mar. Syst.* 28:229–67

Desbruyères D, McDonagh EL, King BA, Thierry V. 2017. Global and full-depth ocean temperature trends during the early twenty-first century from argo and repeat hydrography. *J. Clim.* 30:1985–97

Dewar WK, Bingham RJ, Iverson R, Nowacek DP, St. Laurent LC, Wiebe PH. 2006. Does the marine biosphere mix the ocean? *J. Mar. Res.* 64:541–61

Domingues CM, Church JA, White NJ, Gleckler PJ, Wijffels SE, et al. 2008. Improved estimates of upper-ocean warming and multi-decadal sea-level rise. *Nature* 453:1090–93

Dufresne JL, Bony S. 2008. An assessment of the primary sources of spread of global warming estimates from coupled atmosphere–ocean models. *J. Clim.* 21:5135–44

Durack PJ, Gleckler PJ, Landerer FW, Taylor KE. 2014. Quantifying underestimates of long-term upper-ocean warming. *Nat. Clim. Change* 4:999–1005

Elderfield H, Ferretti P, Greaves M, Crowhurst S, McCave I, et al. 2012. Evolution of ocean temperature and ice volume through the mid-Pleistocene climate transition. *Science* 337:704–9

Emile-Geay J, Madec G. 2009. Geothermal heating, diapycnal mixing and the abyssal circulation. *Ocean Sci.* 5:203–17

Emile-Geay J, McKay NP, Kaufman DS, Von Gunten L, Wang J, et al. 2017. A global multiproxy database for temperature reconstructions of the common era. *Sci. Data* 4:170088

Emiliani C. 1955. Pleistocene temperatures. *J. Geol.* 63:538–75

Feistel R, Wagner W. 2005. High-pressure thermodynamic Gibbs functions of ice and sea ice. *J. Mar. Res.* 63:95–139

Feistel R, Wagner W. 2006. A new equation of state for H_2O ice Ih. *J. Phys. Chem. Ref. Data* 35:1021–47

Ferrari R, Wunsch C. 2009. Ocean circulation kinetic energy: reservoirs, sources, and sinks. *Annu. Rev. Fluid Mech.* 41:253–82

Galbraith ED, Merlis TM, Palter JB. 2016. Destabilization of glacial climate by the radiative impact of Atlantic meridional overturning circulation disruptions. *Geophys. Res. Lett.* 43:8214–21

Gebbie G. 2012. Tracer transport timescales and the observed Atlantic-Pacific lag in the timing of the last Termination. *Paleoceanography* 27:PA3225

Gebbie G. 2014. How much did Glacial North Atlantic Water shoal? *Paleoceanography* 29:190–209

Gebbie G, Huybers P. 2011. How is the ocean filled? *Geophys. Res. Lett.* 38:L06604

Gebbie G, Huybers P. 2012. The mean age of ocean waters inferred from radiocarbon observations: sensitivity to surface sources and accounting for mixing histories. *J. Phys. Oceanogr.* 42:291–305

Gebbie G, Huybers P. 2019. The Little Ice Age and 20th-century deep Pacific cooling. *Science* 363:70–74

Gebbie G, Peterson CD, Lisiecki LE, Spero HJ. 2015. Global-mean $\delta^{13}C$ and its uncertainty in a glacial state estimate. *Quat. Sci. Rev.* 125:144–59

Gleckler PJ, Durack PJ, Stouffer RJ, Johnson GC, Forest CE. 2016. Industrial-era global ocean heat uptake doubles in recent decades. *Nat. Clim. Change* 6:394–98

Gleckler PJ, Wigley TML, Santer BD, Gregory JM, AchutaRao K, Taylor KE. 2006. Volcanoes and climate: Krakatoa's signature persists in the ocean. *Nature* 439:675

Gouretski V, Koltermann K. 2004. *WOCE Global Hydrographic Climatology*. Tech. Rep. 35, Bundesamtes Seeschifffahrt Hydrogr., Hamburg, Ger.

Gregory JM. 2000. Vertical heat transports in the ocean and their effect on time-dependent climate change. *Clim. Dyn.* 16:501–15

Gregory JM, Forster PM. 2008. Transient climate response estimated from radiative forcing and observed temperature change. *J. Geophys. Res. Atmos.* 113:D23105

Haine TWN, Hall TM. 2002. A generalized transport theory: water-mass composition and age. *J. Phys. Oceanogr.* 32:1932–46

Haine TWN, Zhang H, Waugh DW, Holzer M. 2008. On transit-time distributions in unsteady circulation models. *Ocean Model.* 21:35–45

Hakim GJ, Emile-Geay J, Steig EJ, Noone D, Anderson DM, et al. 2016. The last millennium climate reanalysis project: framework and first results. *J. Geophys. Res. Atmos.* 121:6745–64

Huang RX. 2010. *Ocean Circulation: Wind-Driven and Thermohaline Processes*. Cambridge, UK: Cambridge Univ. Press

Huybers P, Curry W. 2006. Links between annual, Milankovitch and continuum temperature variability. *Nature* 442:329–32

IOC (Intergov. Oceanogr. Comm.), SCOR (Sci. Comm. Ocean. Res.), IAPSO (Int. Assoc. Phys. Sci. Oceans). 2010. *The international thermodynamic equation of seawater – 2010: calculation and use of thermodynamic properties*. Man. Guides 56, UN Educ. Sci. Cult. Organ., Paris

Ishii M, Fukuda Y, Hirahara S, Yasui S, Suzuki T, Sato K. 2017. Accuracy of global upper ocean heat content estimation expected from present observational data sets. *Sola* 13:163–67

Jayne SR, St. Laurent LC. 2001. Parameterizing tidal dissipation over rough topography. *Geophys. Res. Lett.* 28:811–14

Johnson GC, Lyman JM, Loeb NG. 2016. Improving estimates of Earth's energy imbalance. *Nat. Clim. Change* 6:639–40

Joyce T. 1986. The geothermal heating of the abyssal subarctic Pacific Ocean. *Deep-Sea Res. I* 33:1003–15

Kennedy J, Rayner N, Smith R, Parker D, Saunby M. 2011. Reassessing biases and other uncertainties in sea surface temperature observations measured in situ since 1850: 2. Biases and homogenization. *J. Geophys. Res. Atmos.* 116:D14104

Khatiwala S, Visbeck M, Schlosser P. 2001. Age tracers in an ocean GCM. *Deep-Sea Res. I* 48:1423–41

Kurahashi-Nakamura T, Paul A, Losch M. 2017. Dynamical reconstruction of the global ocean state during the Last Glacial Maximum. *Paleoceanography* 32:326–50

Lambeck K, Rouby H, Purcell A, Sun Y, Sambridge M. 2014. Sea level and global ice volumes from the Last Glacial Maximum to the Holocene. *PNAS* 111:15296–303

Levermann A, Clark PU, Marzeion B, Milne GA, Pollard D, et al. 2013. The multimillennial sea-level commitment of global warming. *PNAS* 110:13745–50

Levitus S, Antonov JI, Boyer TP, Baranova OK, Garcia HE, et al. 2012. World ocean heat content and thermosteric sea level change (0–2000 m), 1955–2010. *Geophys. Res. Lett.* 39:L10603

Lin L, Khider D, Lisiecki LE, Lawrence CE. 2014. Probabilistic sequence alignment of stratigraphic records. *Paleoceanography* 29:976–89

Loeb NG, Lyman JM, Johnson GC, Allan RP, Doelling DR, et al. 2012. Observed changes in top-of-the-atmosphere radiation and upper-ocean heating consistent within uncertainty. *Nat. Geosci.* 5:110–13

Loeb NG, Thorsen TJ, Norris JR, Wang H, Su W. 2018. Changes in Earth's energy budget during and after the pause in global warming: an observational perspective. *Climate* 6:62

Lueck R, Reid R. 1984. On the production and dissipation of mechanical energy in the ocean. *J. Geophys. Res. Oceans* 89:3439–45

Lyman JM, Good SA, Gouretski VV, Ishii M, Johnson GC, et al. 2010. Robust warming of the global upper ocean. *Nature* 465:334–37

Marchitto T, Bryan S, Doss W, McCulloch M, Montagna P. 2018. A simple biomineralization model to explain Li, Mg, and Sr incorporation into aragonitic foraminifera and corals. *Earth Planet. Sci. Lett.* 481:20–29

Marchitto T, Curry W, Lynch-Stieglitz J, Bryan S, Cobb K, Lund D. 2014. Improved oxygen isotope temperature calibrations for cosmopolitan benthic foraminifera. *Geochim. Cosmochim. Acta* 130:1–11

Marcott SA, Bauska TK, Buizert C, Steig EJ, Rosen JL, et al. 2014. Centennial-scale changes in the global carbon cycle during the last deglaciation. *Nature* 514:616–19

Marshall J, Scott JR, Armour KC, Campin JM, Kelley M, Romanou A. 2015. The ocean's role in the transient response of climate to abrupt greenhouse gas forcing. *Clim. Dyn.* 44:2287–99

Martin P, Lea D, Rosenthal Y, Shackleton N, Sarnthein M, Papenfuss T. 2002. Quaternary deep sea temperature histories derived from benthic foraminiferal Mg/Ca. *Earth Planet. Sci. Lett.* 198:193–209

McDougall TJ. 2003. Potential enthalpy: a conservative oceanic variable for evaluating heat content and heat fluxes. *J. Phys. Oceanogr.* 33:945–63

McDuff R. 1985. The chemistry of interstitial waters, Deep Sea Drilling Project Leg 86. In *Initial Reports of the Deep Sea Drilling Project*, Vol. 86, ed. GR Heath, LH Burckle, pp. 675–87. Washington, DC: US Gov. Print. Off.

McGregor HV, Evans MN, Goosse H, Leduc G, Martrat B, et al. 2015. Robust global ocean cooling trend for the pre-industrial Common Era. *Nat. Geosci.* 8:671–77

Meyssignac B, Boyer T, Zhao Z, Hakuba MZ, Landerer FW, et al. 2019. Measuring global ocean heat content to estimate the earth energy imbalance. *Front. Mar. Sci.* 6:432

Miller MD, Simons M, Adkins JF, Minson SE. 2015. The information content of pore fluid $\delta^{18}O$ and $[Cl^-]$. *J. Phys. Oceanogr.* 45:2070–94

Mitchell LE, Brook EJ, Sowers T, McConnell J, Taylor K. 2011. Multidecadal variability of atmospheric methane, 1000–1800 CE. *J. Geophys. Res. Biogeosci.* 116:G02007

Mouchet A, Deleersnijder E. 2008. The leaky funnel model, a metaphor of the ventilation of the world ocean as simulated in an OGCM. *Tellus A* 60:761–74

Muglia J, Skinner LC, Schmittner A. 2018. Weak overturning circulation and high Southern Ocean utilization maximized glacial ocean carbon. *Earth Planet. Sci. Lett.* 496:47–56

Munk W, Wunsch C. 1998. Abyssal recipes II: energetics of tidal and wind mixing. *Deep-Sea Res. I* 45:1977–2010

Murray J. 1895. *A Summary of the Scientific Results Obtained at the Sounding, Dredging and Trawling Stations of H.M.S. Challenger*, Vol. 1. Edinburgh: H.M. Station. Off.

Myhre G, Shindell D, Bréon F, Collins W, Fuglestvedt J, et al. 2013. Anthropogenic and natural radiative forcing. In *Climate Change 2013: The Physical Science Basis. Contribution of Working Group I to the Fifth Assessment Report of the Intergovernmental Panel on Climate Change*, ed. TF Stocker, D Qin, G-K Plattner, M Tignor, SK Allen, et al., pp. 659–740. Cambridge, UK: Cambridge Univ. Press

Oppo DW, Rosenthal Y, Linsley BK. 2009. 2,000-year-long temperature and hydrology reconstructions from the Indo-Pacific warm pool. *Nature* 460:1113–16

Paasche Ø, Bakke J. 2010. Defining the Little Ice Age. *Clim. Past Discuss.* 6:2159–75

Palter JB, Griffies SM, Samuels BL, Galbraith ED, Gnanadesikan A, Klocker A. 2014. The deep ocean buoyancy budget and its temporal variability. *J. Clim.* 27:551–73

Parrenin F, Masson-Delmotte V, Köhler P, Raynaud D, Paillard D, et al. 2013. Synchronous change of atmospheric CO_2 and Antarctic temperature during the last deglacial warming. *Science* 339:1060–63

Peixoto J, Oort AH. 1992. *Physics of Climate*. New York: Springer

Primeau F. 2005. Characterizing transport between the surface mixed layer and the ocean interior with a forward and adjoint global ocean transport model. *J. Phys. Oceanogr.* 35:545–64

Purkey SG, Johnson GC. 2010. Warming of global abyssal and deep Southern Ocean waters between the 1990s and 2000s: contributions to global heat and sea level rise budgets. *J. Clim.* 23:6336–51

Purkey SG, Smethie WM Jr., Gebbie G, Gordon AL, Sonnerup RE, et al. 2018. A synoptic view of the ventilation and circulation of Antarctic Bottom Water from chlorofluorocarbons. *Annu. Rev. Mar. Sci.* 10:503–27

Ritz SP, Stocker TF, Severinghaus JP. 2011. Noble gases as proxies of mean ocean temperature: sensitivity studies using a climate model of reduced complexity. *Quat. Sci. Rev.* 30:3728–41

Roemmich D, Gould WJ, Gilson J. 2012. 135 years of global ocean warming between the Challenger expedition and the Argo Programme. *Nat. Clim. Change* 2:425–28

Rosenthal Y, Kalansky J, Morley A, Linsley B. 2017. A paleo-perspective on ocean heat content: lessons from the Holocene and Common Era. *Quat. Sci. Rev.* 155:1–12

Scheen J, Stocker TF. 2020. Glacial ocean over-turning intensified by tidal mixing in a global circulation model. *Earth Syst. Dyn. Discuss.* **https://doi.org/10.5194/esd-2020-30**

Schmittner A, Green J, Wilmes S. 2015. Glacial ocean over-turning intensified by tidal mixing in a global circulation model. *Geophys. Res. Lett.* 42:4014–22

Schrag D, Hampt G, Murray D. 1996. Pore fluid constraints on the temperature and oxygen isotopic composition of the glacial ocean. *Science* 272:1930–32

Shackleton N. 1974. Attainment of isotopic equilibrium between ocean water and the benthonic foraminifera genus *Uvigerina*: isotopic changes in the ocean during the last glacial. In *Les Méthodes Quantitative d'Étude des Variations du Climat au cours du Pléistocène*, ed. J Labeyrie, pp. 203–9. Coll. Int. CNRS Vol. 219. Paris: CNRS

Shackleton N, Lamb H, Worssam B, Hodgson J, Lord A, et al. 1977. The oxygen isotope stratigraphic record of the Late Pleistocene. *Philos. Trans. R. Soc. Lond. B* 280:169–82

Shackleton S, Baggenstos D, Menking J, Dyonisius M, Bereiter B, et al. 2020. Global ocean heat content in the last interglacial. *Nat. Geosci.* 13:77–81

Shackleton S, Bereiter B, Baggenstos D, Bauska T, Brook EJ, et al. 2019. Is the noble gas-based rate of ocean warming during the Younger Dryas overestimated? *Geophys. Res. Lett.* 46:5928–36

Shakun JD, Clark PU, He F, Marcott SA, Mix AC, et al. 2012. Global warming preceded by increasing carbon dioxide concentrations during the last deglaciation. *Nature* 484:49–54

Shakun JD, Lea DW, Lisiecki LE, Raymo ME. 2015. An 800-kyr record of global surface ocean $\delta^{18}O$ and implications for ice volume-temperature coupling. *Earth Planet. Sci. Lett.* 426:58–68

Simms AR, Lisiecki LE, Gebbie G, Whitehouse P, Clark JF. 2019. Balancing the Last Glacial Maximum (LGM) sea-level budget. *Quat. Sci. Rev.* 205:143–53

Sosdian S, Rosenthal Y. 2009. Deep-sea temperature and ice volume changes across the Pliocene-Pleistocene climate transitions. *Science* 325:306–10

St. Laurent L, Simmons H. 2006. Estimates of power consumed by mixing in the ocean interior. *J. Clim.* 19:4877–90

Stein CA, Stein S. 1994. Constraints on hydrothermal heat flux through the oceanic lithosphere from global heat flow. *J. Geophys. Res. Solid Earth* 99:3081–95

Steinhilber F, Beer J, Fröhlich C. 2009. Total solar irradiance during the Holocene. *Geophys. Res. Lett.* 36:L19704

Stenchikov G, Delworth TL, Ramaswamy V, Stouffer RJ, Wittenberg A, Zeng F. 2009. Volcanic signals in oceans. *J. Geophys. Res. Atmos.* 114:D16104

Talley L, Feely R, Sloyan B, Wanninkhof R, Baringer M, et al. 2016. Changes in ocean heat, carbon content, and ventilation: a review of the first decade of GO-SHIP global repeat hydrography. *Annu. Rev. Mar. Sci.* 8:185–215

Trenberth KE, Fasullo JT, Von Schuckmann K, Cheng L. 2016. Insights into Earth's energy imbalance from multiple sources. *J. Clim.* 29:7495–505

Umling N, Oppo D, Chen P, Yu J, Liu Z, et al. 2019. Atlantic circulation and ice sheet influences on upper South Atlantic temperatures during the last deglaciation. *Paleoceanogr. Paleoclimatol.* 34:990–1005

Von Schuckmann K, Palmer M, Trenberth K, Cazenave A, Chambers D, et al. 2016. An imperative to monitor Earth's energy imbalance. *Nat. Clim. Change* 6:138–44

Waelbroeck C, Labeyrie L, Michel E, Duplessy JC, McManus J, et al. 2002. Sea-level and deep water temperature changes derived from benthic foraminifera isotopic records. *Quat. Sci. Rev.* 21:295–305

Waelbroeck C, Paul A, Kucera M, Rosell-Melé A, Weinelt M, et al. 2009. Constraints on the magnitude and patterns of ocean cooling at the Last Glacial Maximum. *Nat. Geosci.* 2:127–32

Wang W, Chengchun Q, Ruixin H. 2006. Mechanical energy input to the world oceans due to atmospheric loading. *Chin. Sci. Bull.* 51:327–30

Warren BA. 2006. The first law of thermodynamics in a salty ocean. *Prog. Oceanogr.* 70:149–67

Waugh DW, Hall TM, Haine TWN. 2003. Relationships among tracer ages. *J. Geophys. Res.* 108:3138

Wijffels S, Roemmich D, Monselesan D, Church J, Gilson J. 2016. Ocean temperatures chronicle the ongoing warming of Earth. *Nat. Clim. Change* 6:116–18

Willis JK, Lyman JM, Johnson GC, Gilson J. 2007. Correction to "Recent cooling of the upper ocean." *Geophys. Res. Lett.* 34:L16601

Wunsch C. 1996. *The Ocean Circulation Inverse Problem*. New York: Cambridge Univ. Press

Wunsch C. 2016. Global ocean integrals and means, with trend implications. *Annu. Rev. Mar. Sci.* 8:1–33

Wunsch C. 2016. Last Glacial Maximum and deglacial abyssal seawater oxygen isotopic ratios. *Clim. Past* 12:1281–96

Wunsch C, Ferrari R. 2004. Vertical mixing, energy, and the general circulation of the oceans. *Annu. Rev. Fluid Mech.* 36:281–314

Wunsch C, Heimbach P. 2008. How long to oceanic tracer and proxy equilibrium? *Quat. Sci. Rev.* 27:637–51

Zanna L, Khatiwala S, Gregory JM, Ison J, Heimbach P. 2019. Global reconstruction of historical ocean heat storage and transport. *PNAS* 116:1126–31

Zhu F, Emile-Geay J, McKay NP, Hakim GJ, Khider D, et al. 2019. Climate models can correctly simulate the continuum of global-average temperature variability. *PNAS* 116:8728–33